Study on heat transfer and fluid flow characteristics with short rectangular plate fin of different pattern

By

Islam Md. Didarul[1], Oyakawa Kenyu [2], Yaga Minoru [3] and Senaha Izuru [4]

Abstract

A detailed experimental investigation of the heat transfer and fluid flow characteristics of finned surfaces was conducted for airflow (Re_L = 6250 ~ 25000) at a flat plate boundary layer and narrow duct corresponding to 200 mm and 20 mm duct height respectively. Short rectangular fins of either aluminum or resin material were attached in 7 × 7 arrays to a heating surface and the fin height, inclination angle and fin pattern (co-angular and zigzag) were varied. The fin spacing to length ratios along the streamwise and spanwise directions were kept at S_x/L = 2 and S_z/L = 1, respectively. T-type thermocouples and an infrared camera with a 160 × 120-point In-Sb sensor were used to measure the wall temperature and the detailed heat transfer at the endwall along with fin base. Dye flow in a water channel and titanium oxide oil film flow patterns around the fins were observed to study the flow behavior and its effect on heat transfer. In case of co-angular pattern flow stagnated in front of the fin and formed a strong horseshoe vortex around the fin while the longitudinal vortexes generated by the side top edges touched the fin surface and the endwall. On the other hand in case of zigzag pattern a weak horse shoe vortex appeared in front of the fin while the longitudinal vortex struck the endwall mainly and a sinusoidal wavy flow behavior was observed.

The friction factor value was found to be almost constant and somewhat larger for a zigzag pattern of fins than for a co-angular pattern. The heat transfer results show that a narrow rectangular duct of 20 mm height with fin arrays in a zigzag pattern is the most effective, exhibiting a heat transfer enhancement at the endwall of more than four times over the case without fins wherein co-angular is the least recommended as it exhibits enhancement about a factor of more than three times. At flat plate boundary layer, i.e. in tall duct case both co-angular and zigzag patterns show almost same overall heat transfer enhancement about a factor of three times over the case without fins.

Keywords: Convective heat transfer, Heat transfer enhancement, Rectangular plate fin, Longitudinal vortex, Horseshoe vortex, Infrared image.

1. Introduction

The need for more efficient cooling techniques of devices has recently prompted study into heat transfer and flow characteristics of various configurations of finned surfaces. The pin fin is a typical configuration that is often used to cool the trailing edge region of turbine blades; the internal passage of turbine blades can be very narrow, so that the choice of cooling scheme is limited. The effective heat transfer of staggered arrays of short pin fins was studied by Vanfossen [1] and found to be half that for longer

pin fins. However, this study did not detail the local characteristics of pin fin arrays. Sparrow et al. [2] investigated the local heat transfer coefficient over a plate surface by the naphthalene sublimation technique for a two-row plate fin and tube heat exchanger, finding that the coefficient was lowest behind the pin. The effect of pin fin arrangement on heat transfer over an endwall, the heating surface where the fins are attached, was examined using a thermo sensitive liquid crystal film by Matsumoto et al. [3], who concluded that the heat transfer from the endwall was enhanced by flow acceleration between the pin fins rather than the horseshoe vortex around the pin. Recently, heat transfer enhancement has been reported in studies of an inclined rectangular plate attached to an endwall as an effective vortex generator, wherein a longitudinal vortex is produced with intensity far downstream. It is expected that the heat transfer from an endwall can be improved and hence we have identified this configuration as being very promising. Oyakawa et al. [4] studied the heat transfer of plate setting rectangular fins with an inclination angle of 20° and showed that this configuration can enhance heat transfer. Sparrow et al. [5, 6] studied the heat transfer and pressure drop characteristics of arrays of rectangular modules found in electronic equipment and determined the thermal behavior of the arrays in different situations. Molki et al. [7] experimentally studied the heat transfer at the entrance region of an array of rectangular heated blocks

and presented empirical correlations of the heat transfer for the array. Turk and Junkhan [8] measured the spanwise heat transfer downstream of a rectangular fin mounted on a flat plate. El-Saed et al. [9] investigated heat transfer and fluid flow in rectangular fin arrays and found that the averaged Nusselt number increases with increasing Reynolds number, inter-fin space and fin thickness but did not examine endwall heat transfer. In contrast to rectangular fins, cylinder-like pin fins have been found to exhibit a large pressure drop due to the drag force and flow acceleration or deceleration through the fins. This difference is due to the fact that rectangular arrays do not form extremely narrow passages, which also causes the heat transfer for rectangular fins to be relatively lower. However, the poor heat transfer region behind the pin may be improved by longitudinal vortexes generated by the fin. Furthermore, when the fin array is set such that the inclination angle of every row is changed alternately, the longitudinal vortex produced by the top edge of the fin reattaches to that of the following fin increasing the heat transfer from the fin surface. As the fluid moves, it forms a sinusoidal wave [10] and has considerable contact with the endwall. We also expect that the heat transfer from an endwall can be increased. Igarashi [11] studied heat transfer from a square prism with different inclination angles and observed reattachment flow for inclination angles of 14°–35°. Bilen et al [12] investigated heat transfer enhancement from a

surface fitted with rectangular blocks at different inclination angle and found that the maximum heat transfer was obtained at an inclination angle of 45°, though the local heat transfer characteristics were not reported.

As the above literature review shows, previous studies have investigated heat transfer enhancement from surfaces with arrays of short rectangular fins and a few studies have concentrated on heat transfer from endwalls for short rectangular fins with different inclination angles. However, a detailed discussion about heat transfer from an endwall with arrays of short rectangular fins of different patterns (co-angular and zigzag) in a narrow duct and for a flat plate boundary layer has not yet been completed. Bilen et al. [12] has conducted a study for the co-angular case only, but did not clarify the local heat transfer characteristics. Therefore, we have investigated the heat transfer enhancement for fin arrays on a flat plate boundary layer, i.e. tall duct of 200 mm height and for a narrow duct of 20 mm height by setting short rectangular plates on a duct wall.

In this study we discussed the detailed heat transfer characteristics of fin base and endwall surfaces for different fin patterns and examine the extended surface effect from the fin surfaces and the vortex effect on the endwall for varying fin height and inclination angle. In order to determine the local heat transfer coefficients for a smooth surface, the effects of inclination angle and fin height on the heat transfer enhancement

are measured by the thermocouples on the heating surface. To counteract scatter in the data due to the thermocouples deflection, we also discuss the detailed heat transfer coefficients using infrared images, as the average heat transfer coefficient can be more accurately estimated from an infrared image of a representative fin region. The flow behavior around the fins is also discussed to determine the relation between heat transfer and fluid flow characteristics.

2. Experimental apparatus and procedure

Experiments were conducted in long rectangular ducts both of 20 and 200 mm height, 230 mm span width and 784 mm length. The first row of fins was located 200 mm away from the duct entrance. The experimental apparatus and fin settings are shown in Fig. 1. The fins were made of either aluminum or resin materials and were rectangular type with dimensions 20 mm long, 5 mm thick and three heights, 5, 10 and 15 mm. The fins were set in lines and rows of seven each. The ratios of the fin spacing S_x, S_z to fin length L were set at $S_x/L = 2$ in the streamwise and $S_z/L = 1$ the spanwise direction. The inclination angles of the fins to the flow direction were maintained at α = 0°, 20° and 25°. The fins were attached to the lower wall of the duct by means of a 100 μm double sided thin tape. The upper plate of duct was made of a transparent acrylic

resin plate for observation of the interior of the duct. In the co-angular pattern the fins are set at the same angle in the same direction. In the zigzag pattern the fins have the same angle but are set in alternate directions after each row. The fin setting is illustrated in Figs. 2(a) and (b). As shown in Fig. 1(a) for a duct height of W = 200 mm, the velocity field does not develop over the test section, but rather it assumes fins are in flat plate boundary layer. On the other hand, at W = 20 mm the flow is fully developed.

To measure the local heat transfer coefficients, the lower wall was formed of a Bakelite plate of thickness 10 mm and then attached a 30 μm thick stainless steel foil (200 mm × 784 mm) as a heating surface. A constant heat flux $\dot{q}$ was formed at the heating surface using a direct current source. To prevent heat loss from the heating surface through the lower wall, glass wool was filled in the hollow space and two layers of foam of thickness 60 mm were placed under the Bakelite plate as shown in Fig. 1(c). The wall temperature t_{wx} was measured using 70 μm diameter T-type thermocouples, soldered on the back side of the stainless steel foil attached on the lower wall, at 58 discrete locations along the centerline of the heating surface and the midline between the fins in the spanwise direction, as shown in Fig. 1(a). Moreover, in order to observe the distributions of the temperature and the heat transfer coefficients around the fins at the endwall, infrared images were taken using an infrared camera with a

indium-antimony (In-Sb) sensor, which can measure the temperature at 160×120 points with a resolution of 0.025ºC for a black body. The infrared image measurement is shown in Fig.1 (d). In this case, the temperature was measured at the back of the stainless steel foil through a window covered with two layers of polyvinyledene film with a transmissivity for infrared energy of nearly unity. The back of the stainless steel foil was painted black and the whole experimental apparatus was covered with black cloth to ensure that the surroundings were completely dark.

First, we measured the heat transfer using the thermocouples in the larger region to determine the effect of the fin setting. We then estimated the detailed heat transfer and averaged Nusselt number in the representative region from the infrared images.

In order to determine the basic flow pattern around the rectangular fin, the fluid flow was visualized at lower Reynolds number by inducing fluorescence in the water channel which was made of transparent acrylic plate and of 5 cm height and 50 cm length. Titanium oxide oil film flow patterns at the endwall around the fins in the narrow duct were also observed at Reynolds number similar to that of the main experiment flow. In this experiment, a thin black film was attached to the endwall and black painted fins were attached to the film. The endwall and the fin surface was painted

by a mixture of titanium oxide, linseed oil and oleic acid of suitable density and thenexposed to air flow. To measure the pressure drop resulting from the presence of the fin, 0.5 mm diameter static pressure taps were placed at various locations on the pressure plate. The experiments for the air flow were performed for Reynolds numbers in the range 6250 to 25000 (U = 5 ~ 20 m/s), in the case of flat plate boundary layer based on the mean velocity in the duct and the fin length as representative of the velocity and length respectively.

3. Data reduction

In this study we investigated the fluid flow and heat transfer. The essential quantities determined were the friction factor and the heat transfer coefficients for the different fin patterns.

The friction factor f was evaluated from the pressure difference between points just upstream and downstream of the fins attached to the heating surface using the Eq.(1)

$$f = P_{loss} (D_H/l)/ (\rho_a U^2/2), \quad (1)$$

where l is the distance between just upstream and downstream of the fins and D_H is the hydraulic diameter of the duct.

The heat transfer coefficients,

$$h_x = \dot{q} / (t_{wx} - t_{bx}), \tag{2}$$

were obtained at each thermocouple location, where t_{bx} is the bulk temperature obtained by adding a temperature rise to the entrance temperature, equivalent to the total amount of heat generated between the start of heating and an arbitrary point of measurement.

We considered two kinds of Reynolds numbers and examined their effects on the heat transfer characteristics at the flat plate boundary layer and the narrow duct with fin arrays. The first is based on the mean velocity and fin length, i.e,

$$Re_L = UL / \nu. \tag{3a}$$

The other is based on the mean velocity and the duct hydraulic diameter and can be expressed as

$$Re_H = UD_H / \nu. \tag{3b}$$

The area- averaged Nusselt number based on fin length can be expressed as

$$\overline{Nu_L} = \bar{h}L / \lambda \tag{4a}$$

and that based on the duct hydraulic diameter can be expressed as

$$\overline{Nu_H} = \bar{h}D_H / \lambda. \tag{4b}$$

4. Uncertainty analysis

The pressure was measured by a digital micro manometer of accuracy ± 0.01 mm of H_2O. The temperature was measured by both the thermocouples using a data logger and the infrared camera. The percentage relative uncertainty in the measured temperature for the thermocouples and the infrared camera were ± 0.25% and ± 1.3% respectively. The percentage relative uncertainty in the measured electric power input was ± 1.4%. The percentage relative uncertainty in the compound variables was found to be ± 0.34% both for the velocity and the Reynolds number and – 3.5% ~ + 2.4% both for the heat transfer coefficient and Nusselt number.

5. Results and discussion

5.1. Flow visualization

5.1.1 Dye flow in water channel

In order to focus the difference in the flow behavior between the case of co-angular and zigzag fin pattern, dye flow in water channel was observed at lower Reynolds number. The dye flow patterns for the co-angular and zigzag patterns are shown in Fig. 3. In the case of the co-angular pattern as shown in Fig. 3(a), the dye flow stagnates in front of the fin and forms a horseshoe vortex around the fin. At the rear of

the fin, the vortex rolls up and rises to join the flow separated from the upstream portion of the fin, where it then shows longitudinal behavior. As the fins are set at an angle, edge effects are observed. The corner edges cause turbulence and enhance flow mixing in the inter fin region along the streamwise direction. The main vortex (m.v.) flows above the fins as shown by the arrow in Fig.3 (a), touching the top of the fins and the sidewall. The horseshoe vortex around the co-angular pattern is very strong as observed at every fin rows that the longitudinal vortex cannot contact the inner portion of the horseshoe vortex and the vicinity of the endwall except for the both side walls of the fins. It causes heat transfer enhancement from the fin surface.

In the case of the zigzag pattern shown in Fig. 3(b), a longitudinal vortex generated by the first fin row touches the front of the second row fin and the endwall around the fin as the weak horseshoe vortex appears. This is the difference of flow behavior for zigzag pattern than that of co-angular pattern. Due to the alternate directions of the fins, the flow direction is changed and the longitudinal vortex strikes the endwall between the second and third row fins which causes to increase the heat transfer from the endwall. The inter fin region in the spanwise direction at the third row is contacted by the main vortex. Beyond this row, the flow advances and touches the following fin and the endwall that cause heat transfer increase from the fin and endwall.

We note that the flow attaches strongly to both sides of the fin for the co-angular pattern, while for the zigzag pattern the front side is touched strongly but the back side is lightly touched. Therefore, heat transfer from the fin might be significant in the co-angular case, while heat transfer from the endwall might be higher in the case of the zigzag pattern, as will be compared with infrared image in detailed heat transfer analysis section.

5.1.2 Surface oil film flow patterns around fins at endwall

To compare the flow behavior at the endwall for different fin pattern with the heat transfer from the endwall, oil titanium oxide film flow was observed at higher Reynolds number. The titanium oxide oil film flow patterns at the endwall for the co-angular and zigzag patterns are shown in Fig. 4. An oil film flow pattern at the endwall for the co-angular pattern is shown in Fig. 4(a). In this case for every fin row a horseshoe vortex was clearly observed in front of the fins. A streak line separated from the mid position of the first row fin is observed which then reattached at the back of the fins where the vortex rolled up along the trailing edge of the fin. A longitudinal vortex generated by the side top edge was also observed, which reattached to the inter fin region but could not touch the endwall shielded by the horseshoe vortex and that was

previously observed in dye flow. Another streak line shown in Fig. 4(a) also indicates that the flow passed somewhat diagonally through the passage between the following fins. In this instance it was observed that flow contacted both sides of the fins which causes heat transfer enhancement from the fin surfaces.

Fig. 4(b) shows the flow pattern at the endwall around the zigzag pattern where it looks somewhat different than that of co-angular pattern. Here a horseshoe vortex was also clearly observed but the strength of the vortex appeared to decrease somewhat at the downstream side fins as observed from detached oil film. The longitudinal vortex generated by the side top edges touched the front side of the fins and the nearby endwall. The rear side of the fins was lightly touched which is different than co-angular case. As the directions of the fins alternated, flow could not pass diagonally, but rather flowed in a sinusoidal pattern. It led to increase heat transfer from the endwall. We will discuss later how this flow behavior affects the heat transfer from the endwall with the aid of infrared images.

5.2. Friction factor

The distribution of the local static pressure for the co-angular and zigzag patterns for duct heights of W = 200 mm and 20 mm are shown in Figs. 5(a) and (b),

respectively, in the form of C_p. The pressure distributions measured at the midline decreases in the entrance region and increases in front of the fins for both patterns as shown in Fig. 5(a) and (b). Both the graph shows that the distributions subsequently attain a maximum value and then decrease to a minimum value due to the acceleration of the flow through the space between the fins. After passing the seventh row fins, the pressure gradually recovers. For W = 200 mm as shown in Fig. 5(a), the flow in the duct is not fully developed, and hence the pressure distribution does not decrease accordingly. In Fig. 5(b) for W = 20 mm, the distribution shows that the pressure decreases linearly in the duct. The pressure drop is larger in the narrow duct, especially for the zigzag pattern. As the zigzag arrangement of fins sets each row in alternate directions, the longitudinal vortex generated by the first row fin strikes the large side wall of the following fin as well as the endwall. As a result, a large drag force is developed and a higher pressure drop occurs. In the case of the co-angular pattern, the flow can smoothly pass without contacting many fins and hence the flow is less disturbed and a lower pressure drop occurs.

Fig. 6 shows the friction factor obtained from Eq. (1) in a narrow duct. In the tall duct (W = 200 mm), a hydrodynamic boundary layer does not fully develop. The f values for both patterns are larger than the skin friction for a smooth duct without fins

for fully developed turbulent flow. As the flow for the zigzag pattern has more contact with the fin surface and endwall and consequently a larger drag force occurs than that of the co-angular pattern, the f value is somewhat higher for the zigzag pattern. f is almost constant regardless of the Reynolds number.

5.3. *Local heat transfer coefficients*

5.3.1. Smooth duct results

The distributions of the local heat transfer coefficients h_x at the endwall without rectangular fins are shown in Fig. 7. To check the accuracy of the heat transfer measurements and to determine the characteristics of both ducts without fins, we measured the local heat transfer coefficient on the smooth duct surface. Fig. 7(a) presents the streamwise distributions of the local heat transfer coefficient along the endwall from the duct entrance in the duct of W = 200 mm for U = 5, 10 and 20 m/s. The distributions gradually decrease in the streamwise direction. Since the duct height was large, both the hydrodynamic and thermal boundary layers were still developing, even at the test section. Due to the rough surface at the duct inlet, acting as a tripping surface, the flow was turbulent. The local Nusselt number, based on h_x and the distance, X from entrance agrees with the equation

$$Nu_x = 0.0296 Re_x^{0.8} Pr^{0.6} \quad (5)$$

for a turbulent boundary layer on a flat plate, as shown by the solid lines in Fig.7 (a). In the figure, the open and solid symbols designate the centerline and the midline, respectively. Both sets of data are equal regardless of spanwise position indicating the two dimensionality of the heating surface. The data shows good agreement with Eq. (5).

The results for the narrow duct are shown in Fig. 7(b). The distributions gradually decrease toward the downstream direction at the lowest Reynolds number. At $Re_H = 2.34 \times 10^4$ and 3.51×10^4, the distribution slowly increases and coincides with the following equation for a fully developed hydrodynamic boundary layer for air flow at the downstream region as shown by the solid lines:

$$Nu_H = 0.019\ Re_H^{0.8}. \quad (6)$$

Hence the duct heights of $W = 200$ mm and $W = 20$ mm represents a flat plate turbulent boundary layer and a fully developed duct flow in test section, respectively.

5.3.2. Effect of inclination angle on heat transfer

The effect of the inclination angle of the rectangular fin on the local heat transfer coefficient is presented in Figs. 8(a), (b), and (c) for $\alpha = 0°$, 20° and 25°, respectively. Each graph represents the streamwise local heat transfer coefficient at the centerline and

at the midline. Fig. 8(a) shows the distribution for $\alpha = 0°$.The data for the centerline decreases gradually up to front of the first row of fins, where it exhibits a rapid increase and attains a maximum value before rapidly decreasing to a minimum value, with the pattern repeated periodically. Maximum values are obtained at fin positions and the minima are obtained between the fins along the streamwise direction. The maximum value at the fin center may be the combined effect of the extended surface and longitudinal vortex. Even the minimum values are higher than those without fins and hence it may be considered that heat transfer is enhanced by turbulence or large scale vortexes generated by the fins. The solid symbols, i.e. the midline distribution as shown in Fig.8 (a) show the heat transfer enhancements at the endwall caused by the longitudinal and other vortexes. Midline distributions are also appeared to be periodical for $\alpha = 0°$ while heat transfer increases between fins in spanwise and decreases at the other places. Though the trends of distribution along centerline for $\alpha = 20°$ (Fig. 8(b)) and 25° (Fig. 8(c)) is found similar to that for $\alpha = 0°$, the heat transfer coefficients along the midline shows somewhat different. Along the midline, the local heat transfer coefficients are affected by the longitudinal vortex, maintaining large values for $\alpha = 20°$ and 25° compared to the case for 0°. It should be mentioned that the thermocouple at the center of the seventh row fin as shown in Fig. 8(a) and (b) was broken and that data was

assumed and shown by dashed line. Comparing the centerline and midline distributions among the three inclination angle heat transfer coefficient for $\alpha = 20°$ is considered highest , which agrees with the data obtained by Bilen et al. [12] who found that the effect of inclination angle on heat transfer enhancement is small for inclination angles larger than 22.5°. An inclination angle of 20° caused considerable enhancement in heat transfer. This is because of the edge effect of the rectangular fin, which increases the flow mixing. When the fins are turned around the mid point, the side edges can produce more turbulence. This situation has been discussed by Herman [13] and Herman and Kang [14]. Therefore, an inclination angle of 20° is preferred for further analysis.

5.3.3 Heat transfer through fin of resin material

We now want to discuss the fin material with regards estimating the effect of a vortex generator on the endwall, not for the extended surface. The local heat transfer coefficient was measured for a resin material fin and the results are presented in Fig. 9. In this figure centerline distribution shows that the heat transfer coefficient at the fin position for resin material in contrast to the aluminum fin as shown in Fig. 8(b) is smaller. The coefficient at the midline also appears to be equal to that of the centerline. So the overall heat transfer may be enhanced by a factor of about two times than that of

without fins. This results in the effect of vortex generator with no effect from extended surface. Because the Biot number for the resin material was estimated 10 and the conduction resistance of resin fin was nearly equal to the thermal resistance. As mentioned, thin double-sided tape of thickness 100 μm was used to attach the fin to the heating surface. For the aluminum fin, the conduction resistance of the tape was 5% of the total resistance (for an average heat transfer coefficient $\bar{h}$ assumed to be 200 W/m^{2}K). Therefore, the tape did not have much affect on the estimation of the heat transfer coefficient from fin. Also, the Biot number, *Bi* of the aluminum fin was about 0.009, which is small enough. Therefore, the heat transfer enhancement by an aluminum fin only will be discussed in the present experiment.

5.3.4 Effect of fin height on heat transfer

The effect of the height of the fin on the local heat transfer coefficient is now discussed. Fig.10 shows the streamwise local heat transfer coefficient distribution for varying fin height in case of co-angular pattern in a flat plate boundary layer as a typical example. It was found that as the fin height increases, the extended surface area also increases and as a consequence the heat transfer rate increases. The local heat transfer coefficient shows a periodic distribution regardless of fin height. The difference in the

heat transfer enhancement between fin heights of 10 mm and 15 mm was comparatively small, while the difference between fins of 5-mm height and other fins was larger. Hence, a 10 mm height fin was chosen as a typical fin in this experiment.

5.3.5 Effect of velocity on heat transfer

The effect of velocity on the local heat transfer coefficient in a duct of 200 mm height for a co-angular pattern is shown in Fig. 11(a). The local heat transfer coefficient slowly decreases in both the upstream and downstream region, while at the finned region a periodic distribution appears, independent of velocity. The distribution for the zigzag pattern is similar to that of the co-angular pattern, as shown in Fig. 11(b), though with some differences. For the zigzag pattern, the heat transfer coefficient profile near the lower peaks appears concave and shows higher values than that of the co-angular pattern. The peak values in the upstream region are higher for the co-angular pattern than for the zigzag pattern. This is because in the case of the co-angular pattern the flow touches both sides of the fins strongly and then continues to downstream smoothly whereas for the zigzag pattern the flow strongly touches the endwall and the front side of the fin while the other side remains softly touched. Thus, the extended surface is more effective in the case of the co-angular pattern for a flat plate boundary layer.

Fig. 11(c) shows the distribution of the heat transfer coefficient for the zigzag pattern in a narrow duct. In this figure the upper peak values are found to be the highest because the upper wall of the narrow duct causes the flow to strike the endwall and the fin more strongly. In this case centerline thermocouple at the first row fin was also broken and the data was assumed as shown by dashed line. Data for the co-angular pattern for the narrow duct is not shown but the distribution was almost the same for the as the tall duct. In Fig. 11(a), (b) and (c), the maximum heat transfer coefficient shows some discrepancy at some streamwise velocities due to small deflections of the thermocouples from the centerline.

5.4 Detailed heat transfer analysis

Detailed heat transfer coefficient distributions at the endwall surfaces for rectangular fins of both co-angular and zigzag patterns for a flat plate boundary and narrow duct flow are shown in Figs. 12–15. As shown in Figs. 12(a) and 13(a), the heat transfer is high around the fin rows for both patterns. Comparing the values of h_x between the two patterns shows that the higher heat transfer regions increases for zigzag pattern. In the co-angular pattern, the horseshoe vortex is responsible for the enhancement of the heat transfer around the fins. The heat transfer in the region

between fins in the spanwise direction is also enhanced due to lateral mixing, as explained by Herman [13]. In the zigzag pattern, the horseshoe vortex as well as the vortex generated by the side top and corner edges strongly touches the alternately angled fin surfaces and endwall, which significantly enhances the heat transfer.

Figs. 12(b) and 13(b) show the heat transfer distribution along the centerline and midline. For both patterns, the centerline distribution is periodic and each peak indicates the h_x value at the fin center. Around the third row fins the distributions show higher values of h_x, followed by a subsequent decline in the downstream side fins. The slope of the decline is greater for the co-angular pattern than for the zigzag pattern. The midline distribution, showing the endwall heat transfer, looks flat and is nearly half the maximum value. It is also notable that the slope of the decline is again higher for the co-angular pattern. The lesser slope for the zigzag pattern might be due to the vortex flow that strongly attaches to the farthest row fin. Figs. 12(c) and 13(c) show the spanwise distribution for both patterns. The trends of the distributions are similar, but the values of h are different. At X^*/L = 0, 2 and 4, i.e. at the center of each fin row, periodic distributions appear. At the upstream side fins the lower peak and higher peak values are higher for the co-angular pattern, but at the downstream side fins the zigzag pattern exhibit higher values. At X^*/L = 0.5 and 2.5, the distributions tend towards being

flat while at X^*/L = 1 and 3, they become almost flat. Immediately before the fins, i.e. at X^*/L = 1.5 and 3.5, the distributions become periodic again.

Figs. 14 and 15 show the distributions for the narrow duct flow. A comparison between Figs. 14(a) and 15(a) identifies the different shapes of the heat transfer profile. In the case of the co-angular pattern, the lower heat transfer regions are comparatively large and hysterisis shaped, while for the zigzag pattern, the lower heat transfer regions are comparatively small with a delta shape. In the oil film flow as shown in Fig. 4(b) for the zigzag pattern, the delta-shaped region appears in front of the fins at the endwall, which is not entirely involved in the flow. This corresponds to the delta-shaped lower heat transfer region observed in the infrared image. The horseshoe vortexes around the fin for both patterns observed for the oil film flow agree with the observed higher heat transfer region around the fin in the infrared images. The level of heat transfer increases in a narrow duct compared to a flat plate because the upper wall induces the flow vortex to attach to the endwall and fin surface more strongly. Large higher heat transfer regions around each fin row are observed for both patterns. Figs. 14(b) and 15(b) show the distribution along the centerline and midline. Though the patterns of the distributions are similar to those for the flat plate case, h_x is greater and there is no significant decline. The lower peak profiles are convex for the co-angular pattern, while in contrast the

profile is flat for the zigzag pattern and the lower peaks are comparatively higher. The midline distribution is nearly straight for both patterns but the h_x values are greater for the zigzag pattern. Figs. 14(c) and 15(c) show the spanwise distribution for both patterns. The distribution is almost periodic except at X^*/L = 1 and 3. Both the lower and higher peak profiles are comparatively more convex for the co-angular pattern, while for the zigzag pattern the profiles are higher and somewhat flat.

5.5. Area - averaged heat transfer

The area-averaged heat transfer coefficients at the endwall and for the overall surfaces of the representative third, fourth and fifth row fins were measured from infrared images with the following equation:

$$\bar{h}_{\text{overall}} = \frac{A_{\text{fin}}}{A_{\text{overall}}}\bar{h}_{\text{fin}} + \frac{A_{\text{endwall}}}{A_{\text{overall}}}\bar{h}_{\text{endwall}}, \tag{7}$$

where, A_{overall} is the overall surface area including the fin base, A_{fin} and A_{endwall} is the endwall area. The relationship between the area-averaged Nusselt number and the Reynolds number is shown in Fig. 16. The area-averaged Nusselt number is represented by the curve fitted lines. All the data fall smoothly on the curve fitted lines and can be well represented by the equation.

$$\overline{Nu} = cRe^{0.7}. \tag{8}$$

Values for *c* for different duct heights and fin patterns are listed in Table 1. It is found that the zigzag pattern has higher *c* values. Fig. 16(a) shows the variation of the Nusselt number with the Reynolds number at the endwall and the overall surface for both patterns for a narrow duct, where the Nusselt number is arranged by duct hydraulic diameter. For all cases, the Nusselt number increases with Reynolds number. Considering the overall heat transfer, the zigzag pattern shows a higher value than the co-angular pattern. As noted previously, this is due to the fact that for the zigzag setting the longitudinal vortex strikes the endwall and the fin surface more strongly up to the farthest fin row. Comparing the endwall heat transfer, the difference in the heat transfer between the co-angular and zigzag patterns is more than the difference in that of the overall surface area, indicating that the endwall heat transfer is more significant for the zigzag pattern while the extended surface (fin) effect is significant for the co-angular pattern. The overall heat transfer is found to be enhanced by more than four times the smooth surface value.

The variation in the Nusselt number with Reynolds number at the flat plate boundary layer is shown in Fig. 16(b), with the Nusselt number arranged by fin length. The overall heat transfer enhancement for both fin patterns is nearly the same though the coefficient *c* for the zigzag pattern is somewhat higher. The endwall heat transfer for

the two fin patterns is also similar.

The heat transfer from a smooth surface was estimated as follows: The heat transfer coefficients were first calculated from the Eq. (5) for the flat plate boundary layer within the range X = 0.28 m to 0.36 m, corresponding to the length between the third and fifth rows. These coefficients were then replaced by the average Nusselt number based on fin length, represented by the following equation:

$$\overline{Nu}_{\mathrm{L}} = 0.0138 Re_{\mathrm{L}}^{0.8}. \quad (9)$$

The overall heat transfer was then compared and found to be more than three times the smooth surface value. Hence, it was found that heat transfer is improved with the use of fins. A zigzag pattern for W = 20 mm was found to be the most effective for heat transfer enhancement.

6. Conclusions

We have performed an experimental investigation of extended surface and endwall heat transfer coefficients and fluid flow characteristics in rectangular ducts with short rectangular plate fins. The effects of fin height, inclination angle, fin pattern and Reynolds number were examined and the following conclusions can be drawn**:**

1. The inclination angle has a great influence on the heat transfer enhancement.

Among the inclination angles 0°, 20° and 25°, an angle of 20° appears optimum for enhancement in this experiment.

2. The friction factors for both patterns were larger compared with the skin friction on the smooth surface for a fully developed turbulent flow. The friction factor value was found to be almost constant and larger for a zigzag pattern of fins than for a co-angular pattern.
3. In dye flow in water channel, flow stagnated in front of the fin and formed a strong horseshoe vortex around the fin while the longitudinal vortexes generated by the side top edges touched the fin surface and the endwall in case of co-angular pattern. On the other hand in case of zigzag pattern a weak horse shoe vortex appeared in front of the fin while the longitudinal vortex struck the endwall mainly and a sinusoidal wavy flow behavior was observed.
4. Titanium oxide oil film flow patterns traced out a strong horseshoe vortex around the fins in the co-angular pattern and also showed a diagonal fluid movement that strongly touches both sides of the fins. The fluid flow around the fins in the zigzag pattern clearly indicated a sinusoidal wavy pattern along with a weak horseshoe vortex.
5. Comparing arrays of co-angular and zigzag patterns, the later is more effective for

heat transfer enhancement in the case of the narrow duct flow. The average heat transfer coefficient for a zigzag pattern is more than four times higher than that without fins. The Nusselt number increases with Reynolds number to the 0.7^{th} power for both patterns in a narrow duct as well as for a flat plate boundary layer.

Nomenclature

C_p : pressure coefficient = $2(P-P_\infty)/\rho U^2$

D_H : equivalent diameter of the duct, m

f : friction factor

L : fin length = 20 mm

W : height of duct = 20 and 200 mm

H : height of fin = 5 ~15 mm

$\bar{h}$: average heat transfer coefficient, W/m^{2}K

h : heat transfer coefficient, W/m^{2}K

h_x : streamwise local heat transfer coefficient, W/m^{2}K

$\overline{Nu_L}$: averaged Nusselt number ($\bar{h}L/\lambda$)

$\overline{Nu_H}$: averaged Nusselt number ($\bar{h}D_H/\lambda$)

P, P_∞ : streamwise and atmospheric pressure respectively, N/m^2

t_{bx} : bulk temperature of duct flow, °C

t_{wx} : duct wall surface temperature, °C

Re_H : Reynolds number (UD_H/ν)

Re_L : Reynolds number (UL/ν)

U : mean air velocity, m/s

PR : pitch ratio

S_x : fin spacing in streamwise direction (shown in Fig. 2)

S_z : fin spacing in spanwise direction (shown in Fig. 2)

X : streamwise coordinate (X = 0 at the center of rectangular fin of first row) as illustrated in Fig.1

Z : spanwise coordinate (Z = 0 at the center of rectangular fin of first row) as illustrated in Fig.1

X^* : streamwise coordinate (X^*= 0 at the center of rectangular fin of third row)

Z^* : spanwise coordinate (Z^* = 0 at the center of rectangular fin of third row)

Greek symbols

α : inclination angle

v : kinematic viscosity of air, m^2/s

λ : thermal conductivity, W/mK

Acknowledgements

This research work is supported by Monbukagakusho and Heiwa Nakajima Foundation. This support is gratefully acknowledged.

References

[1] G.J. Van Fossen, Heat transfer coefficients for staggered arrays of short pin ifns, Journal Engineering Power, 104 (1982) 268-274 .

[2] E.M. Sparrow and F.E.M. Saboya, Transfer characteristics of two-row plate fin and tube heat exchanger configurations, International Journal of Heat and Mass Transfer, 19 (1976) 41-49.

[3] Ryosuke Matsumoto, Shinzo Kikkawa and Mamoru Senda, Effect of pin fin arrangement on end wall heat transfer, JSME International Journal Series B, 40(1) (1997) 142-151

[4] K. Oyakawa, Y. Furukawa, T. Taira, I. Senaha, Effect of vortex generators on heat transfer enhancement in a duct, Proceeding of the Experimental Heat Transfer, Fluid Mechanics and Thermodynamics, Honolulu, Hawaii, pp. 633-640, (1993).

[5] E.M. Sparrow, J.E. Niethammer, A. Chaboki, Heat transfer and pressure drop characteristics of arrays of rectangular modules encountered in electronic equipment, International Journal of Heat and Mass Transfer, 25 (1982) 961-973.

[6] E.M. Sparrow, S.B.Vemuri, D.S Kadle, Enhanced and local heat transfer, pressure

drop, and flow visualization for arrays of block-like electronic components, International Journal of Heat and Mass Transfer, 26 (1983) 689-699.

[7] M. Molki, M. Faghri, O. Ozbay, A correlation for heat transfer and wake effect in the entrance region of an inline array of rectangular blocks simulating electronic components, ASME Journal of Heat Transfer, 117 (1995) 40-46.

[8] A.Y. Turk, G.H Junkhan, Heat transfer enhancement downstream of vortex generators on a flat plate, Heat Transfer, C.I. Tien et al. ed., Hemisphere Washington, 6 (1986) 2903-2908.

[9] S.A. El-Saed, S.M. Mohamed, A.M. Abdel-Latif, A.E. Abouda, Investigation of turbulent heat transfer and fluid flow in longitudinal rectangular fin-arrays of different geometries and shrouded fin array, Experimental Thermal and Fluid Science, 26 (2002) 879-900.

[10] K. Oyakawa, I. Mabuchi, The effects of the channel width on heat transfer augmentation in a sinusoidal wave channel, JSME International Journal, Series II, 32 (3) (1989) 403-410.

[11] T. Igarashi, Local heat transfer from a square prism to an air stream, International Journal of Heat and Mass Transfer, 29 (5) (1983) 777-784.

[12] K. Bilen, S. Yapici, Heat transfer from a surface fitted with rectangular blocks at different orientation angle, Journal of Heat Mass Transfer, 38(2002) 649-655.

[13] C. Herman, Experimental visualization of temperature fields and measurement of

heat transfer enhancement in electronic system models, In: S Kakac; H Yuncu; K Hijikata (eds) Cooling of Electronic systems, NATO ASI Series 258, Kluwer Academic, Dedrecht (1994) 313-337

[14] C. Herman, E. Kang, Experimental visualization of temperature fields and study of heat transfer enhancement in oscillatory flow in a grooved channel, Journal of Heat Mass Transfer, 37(2001) 87

Figures caption

Fig.1 Experimental apparatus with fin

(a) Fin with heating surface and Dimensions

(b) Fin inside duct

Fig.2 Arrangement of short rectangular fin

Fig.3 Flow visualization in a water channel around short rectangular fin of (a) co-angular, (b) zigzag pattern with H = 10 mm, PR = 2 and Re_H = 1350

Fig.4 Titanium oxide oil film flow pattern at the endwall around (a) Co-angular pattern and (b) Zigzag pattern for H =10 mm, $Re_H = 4.68 \times 10^4$ in a narrow duct flow.

Fig.5 Pressure drop at co-angular and zigzag pattern for U = 15 m/s, H = 10 mm for (a) flat plate boundary layer (W = 200 mm) and (b) narrow duct flow (W = 20 mm).

Fig.6 Friction factor vs. Reynolds number in a narrow duct for co-angular and zigzag pattern of H = 10 mm

Fig.7 Local heat transfer distributions without fin on smooth surface

Fig.8 Effect of attack angle on local heat transfer coefficients for H = 10 mm, W = 200 mm and U = 10 m/s

Fig.9 Variation of local heat transfer coefficient for resin material with $\alpha = 20^{\circ}$, H = 10 mm, W = 200 mm.

Fig.10. Effect of fin height on local heat transfer coefficient along centerline at co-angular pattern for W = 200 mm and U =10 m/s

Fig.11 Variation of local heat transfer coefficient with velocity along centerline for H = 10 mm

Fig.12 Detailed heat transfer coefficient distributions around the representative fins of

Table caption

Table1. Coefficient of heat transfer correlation

Figure 1

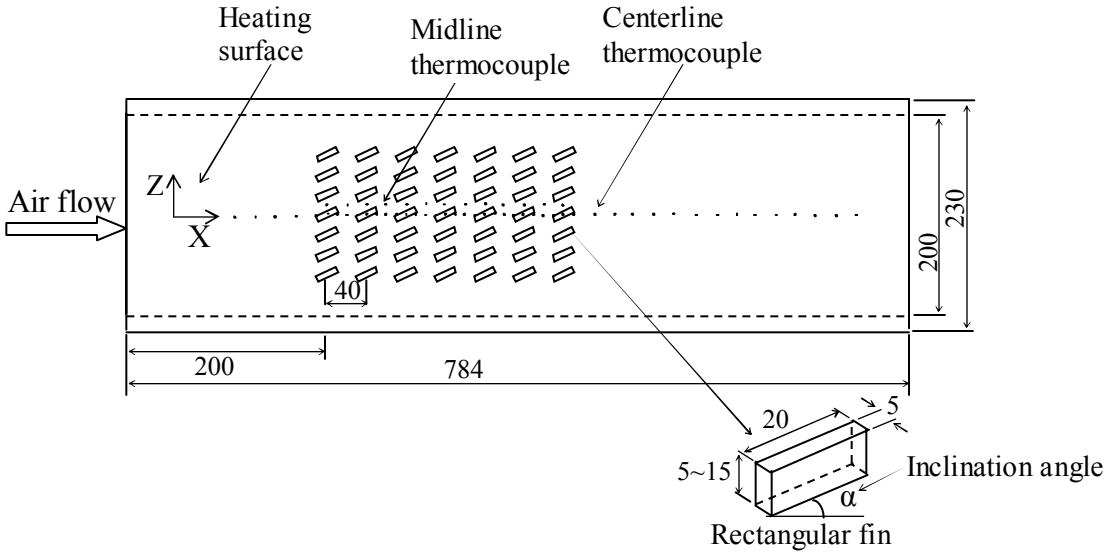

(a) Fin with heating surface and Dimension

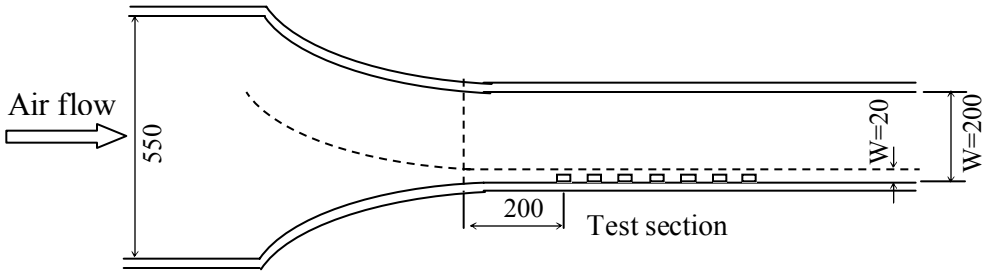

(b) Fin inside duct

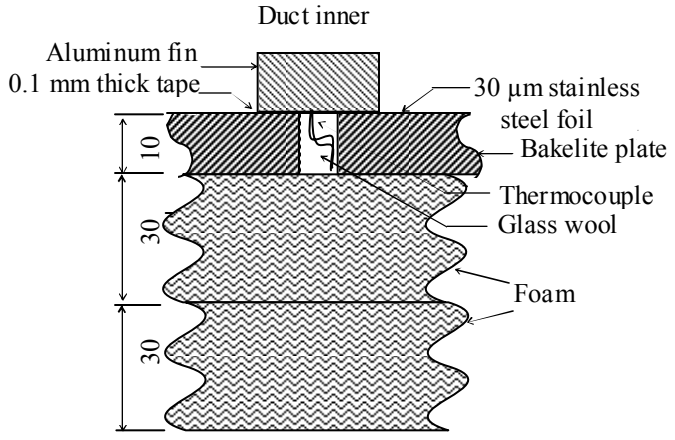

(c) Thermocouple measurement

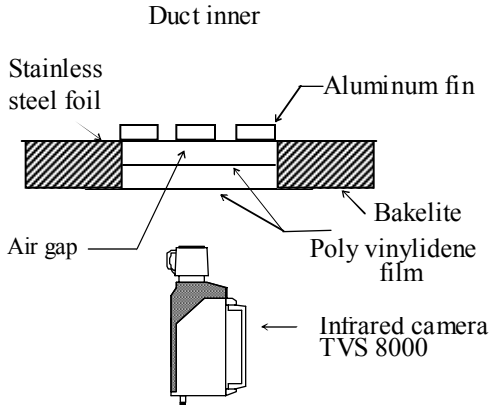

(d) Infrared measurement

Fig.1. Experimental apparatus with fin (all dimensions are in mm)

Figure 2

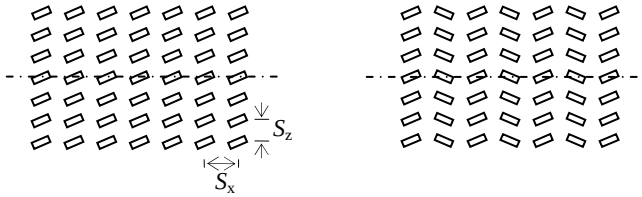

(a) Co-angular pattern (b) Zigzag pattern

Fig. 2. Arrangement of short rectangular fin

Figure 3

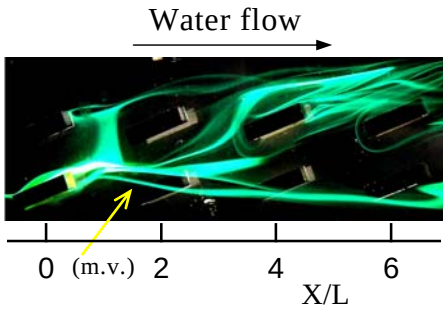

(a) Co-angular pattern

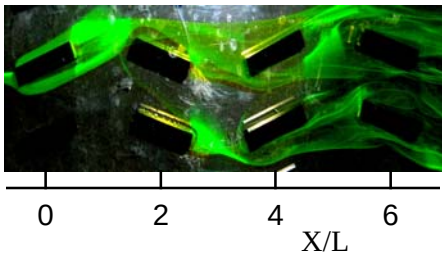

(b) Zigzag pattern

Fig. 3. Flow visualization in a water channel around short rectangular fin of (a) co-angular, (b) zigzag pattern with H = 10 mm, PR = 2 and Re_{H} = 1350.

Figure 4

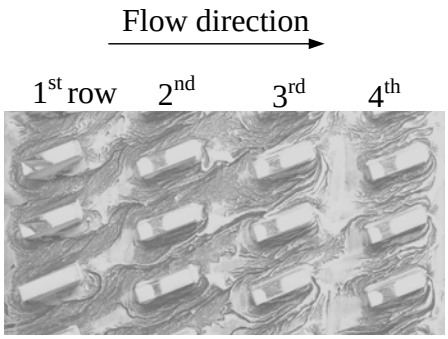

(a) Co-angular pattern

(b) Zigzag pattern

Fig. 4. Titanium oxide oil film flow pattern at the endwall around (a) Co-angular and (b) Zigzag pattern for H =10 mm, $Re_H = 4.68 \times 10^4$ in a narrow duct flow.

Figure 5

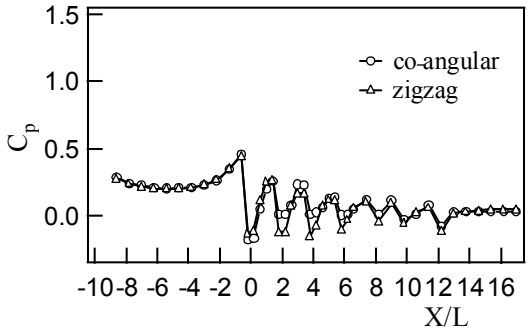

(a) W = 200 mm

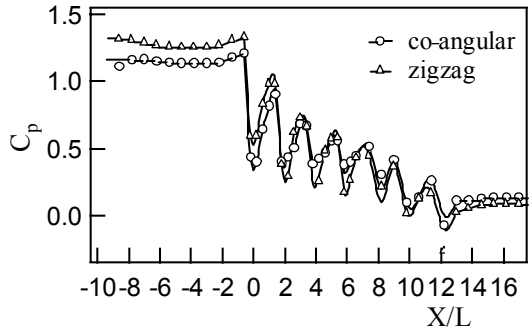

(b) W = 20 mm

Fig. 5. Pressure drop at co-angular and zigzag patterns for $U = 15$ m/s and $H = 10$ mm for a (a) flat plate boundary layer ($W = 200$ mm) and (b) narrow duct flow ($W = 20$ mm)

Figure 6

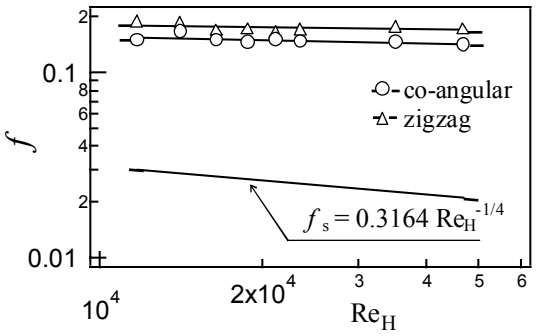

Fig. 6. Friction factor vs. Reynolds number in a narrow duct for co-angular and zigzag pattern of $H = 10$ mm

Figure 7

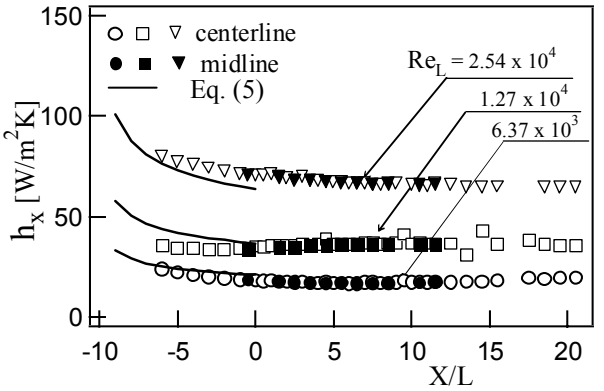

(a) W = 200 mm

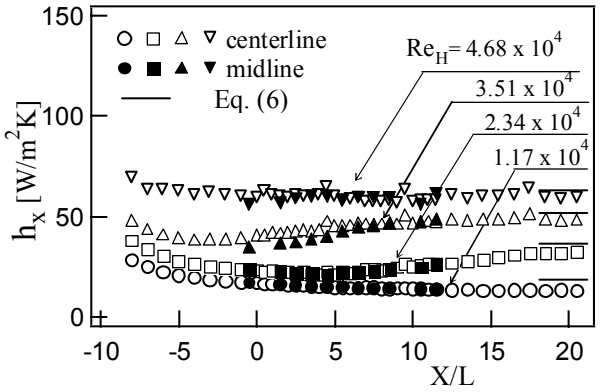

(b) W = 20 mm

Fig. 7. Local heat transfer distributions without fin on smooth surface

Figure 8

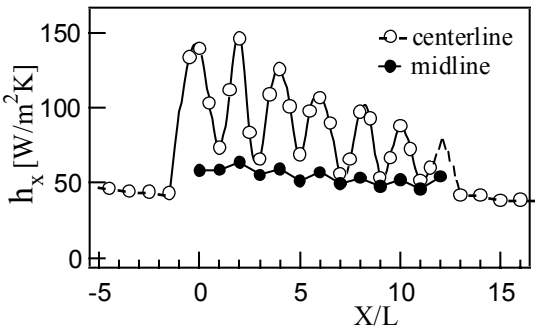

(a) $\alpha = 0^{\circ}$

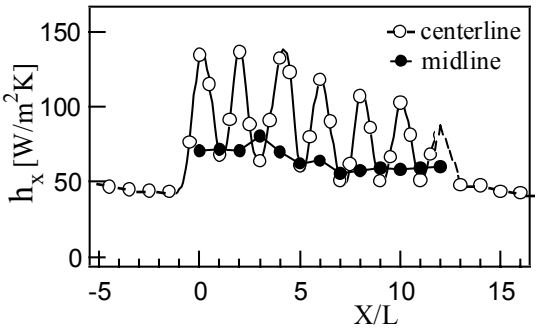

(b) $\alpha = 20^{\circ}$

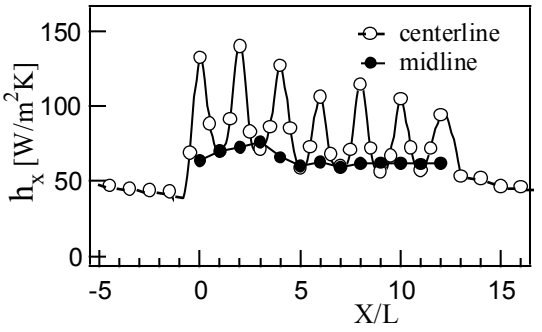

(c) $\alpha = 25^{\circ}$

Fig. 8. Effect of attack angle on local heat transfer coefficients for $H = 10$ mm, $W = 200$ mm and $U = 10$ m/s

Figure 9

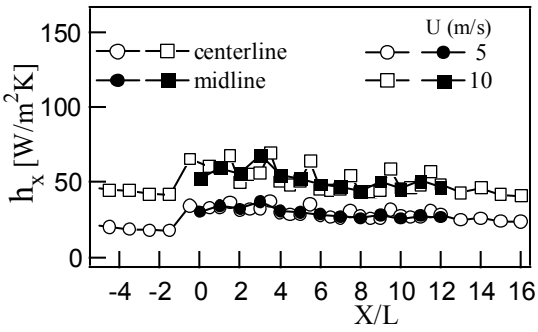

Fig. 9. Variation of local heat transfer coefficients for resin material with $\alpha = 20^{\circ}$, $H = 10$ mm, $W = 200$ mm.

Figure 10

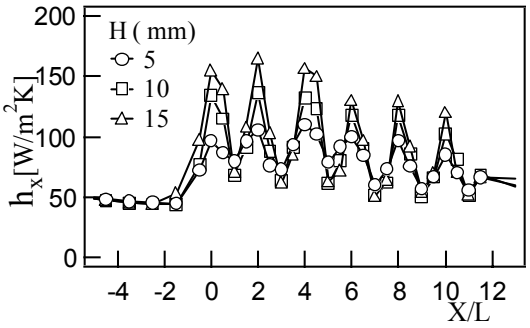

Fig.10. Effect of fin height on local heat transfer coefficient along centerline at co-angular pattern for W = 200 mm and U =10 m/s

Figure 11

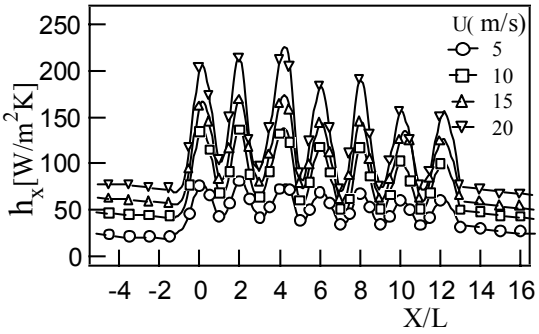

(a) Co-angular pattern, W = 200 mm

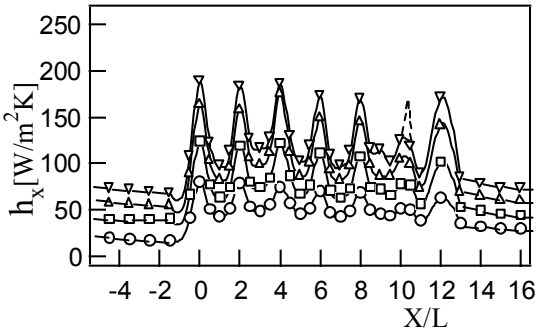

(b) Zigzag pattern, W = 200 mm

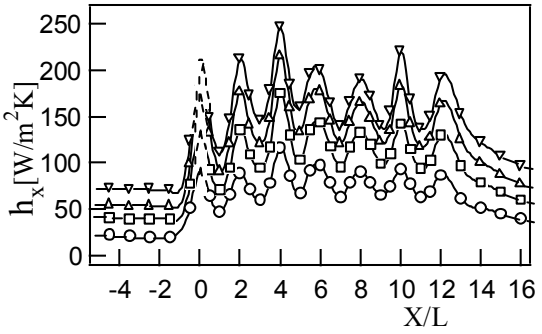

(c) Zigzag pattern, W = 20 mm

Fig. 11. Variation of local heat transfer coefficient with velocity along centerline for H = 10 mm

Figure 12

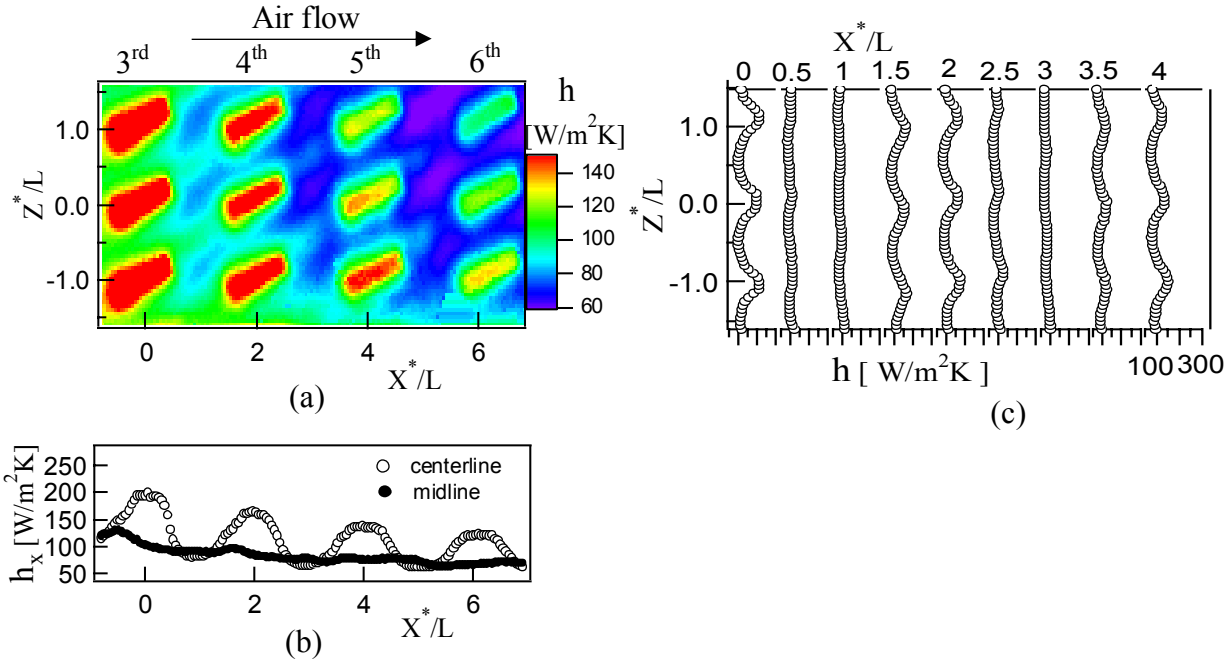

Fig. 12. Detailed heat transfer coefficient distributions around the representative fins of co-angular pattern at the endwall in a flat plate boundary layer ($W = 200$ mm) for $Re_L = 1.27 \times 10^4$, $H = 10$ mm. (a) Infrared image. (b) Centerline and midline distributions and (c) Spanwise distributions.

Figure 13

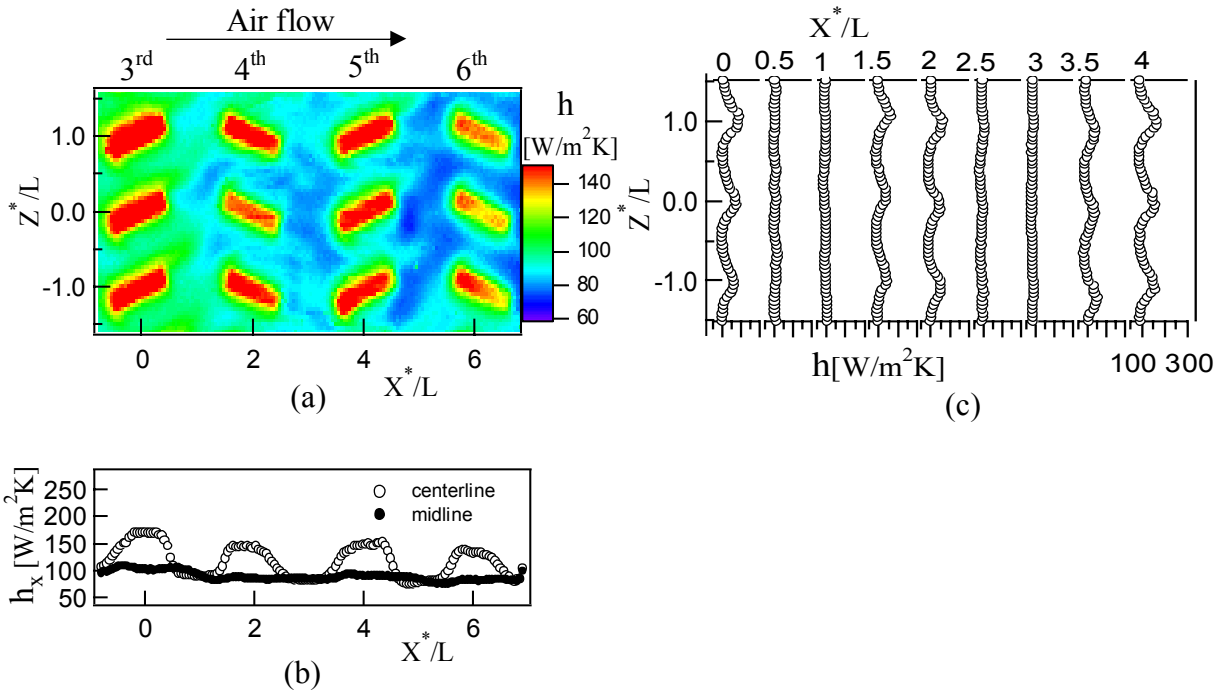

Fig. 13. Detailed heat transfer coefficient distributions around the representative fins of zigzag pattern at the endwall in a flat plate boundary layer (W = 200 mm) for $Re_L = 1.27 \times 10^4$, H = 10 mm. (a) Infrared image. (b) Centerline and midline distribution and (c) Spanwise distribution.

Figure 14

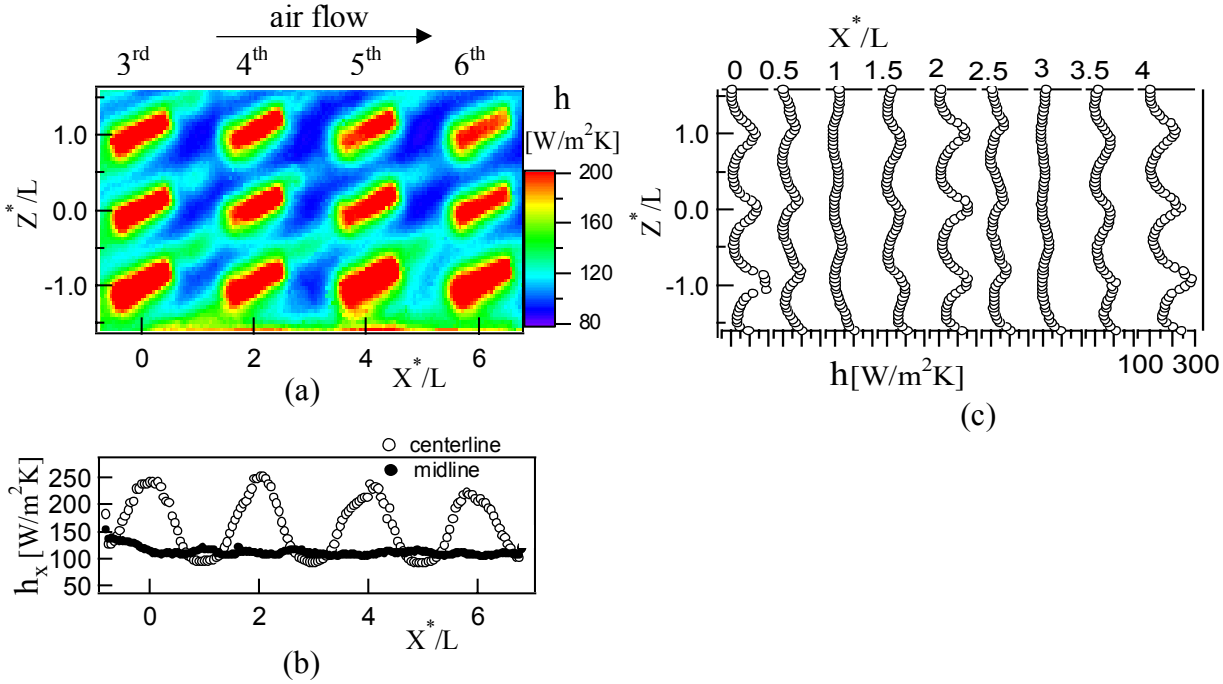

Fig. 14. Detailed heat transfer coefficient distributions around the representative fins of co-angular pattern at the endwall in a duct flow (W = 20 mm) for $Re_H = 2.34 \times 10^4$, H = 10 mm. (a) Infrared image. (b) Centerline and midline distribution and (c) Spanwise distribution.

Figure 15

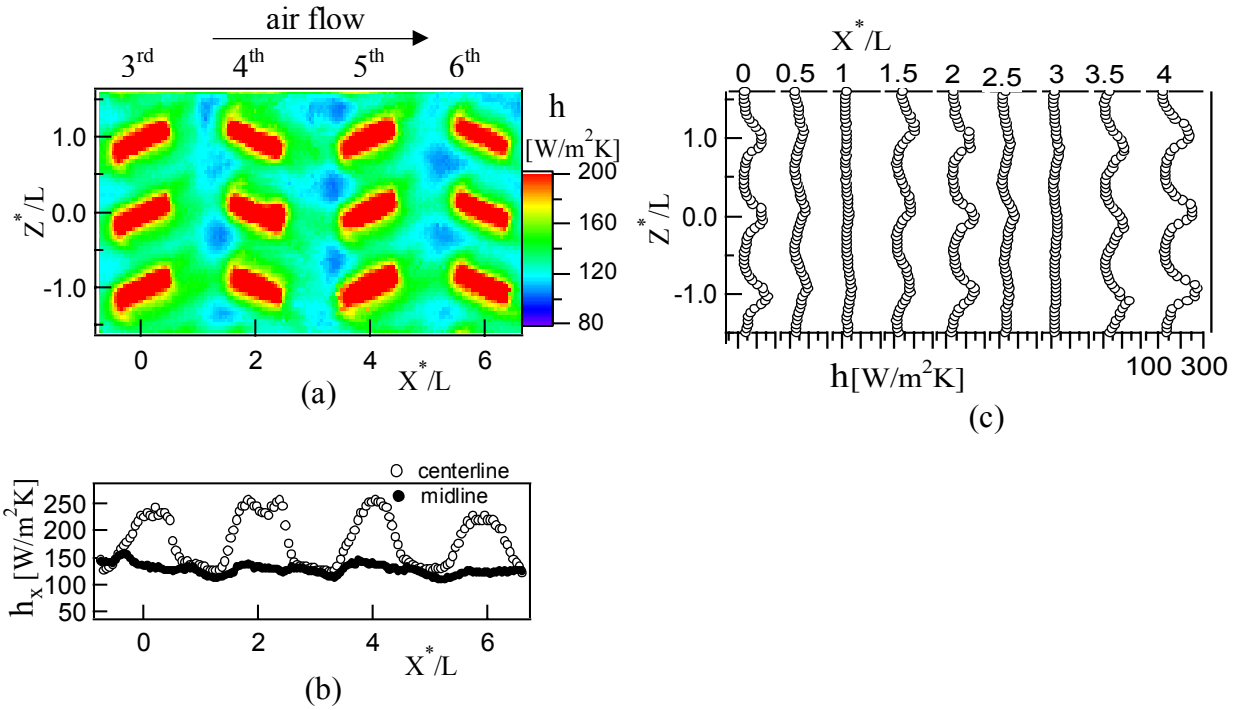

Fig. 15. Detailed heat transfer coefficient distributions around the representative fins of zigzag pattern at the endwall in a duct flow (W = 20 mm) for $Re_H = 2.34 \times 10^4$, H =10 mm. (a) Infrared image. (b) Centerline and midline distribution and (c) Spanwise distribution.

Figure 16

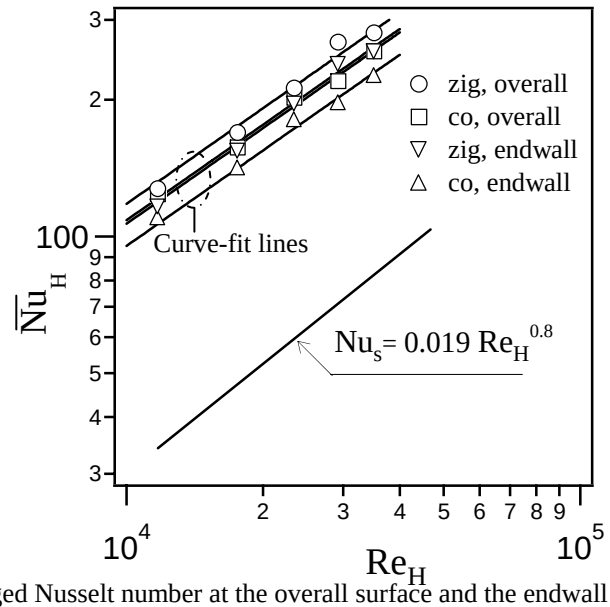

(a) Area–averaged Nusselt number at the overall surface and the endwall as a function of the duct Reynolds number for W = 20 mm.

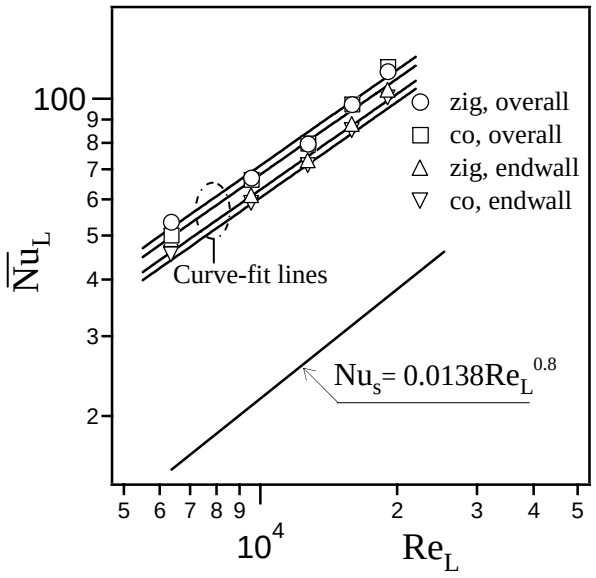

(b) Area–averaged Nusselt number at the overall surface and the endwall as a function of the Reynolds number based on fin length for W = 200 mm.

Fig. 16. Relationship between Nusselt number and Reynolds number

Table 1

Table 1
Coefficient of heat transfer correlations

Fin Pattern	Duct Height (mm)	$\overline{Nu} = cRe^{0.7}$	
		c	
		endwall	overall
Co angular	20	0.151	0.169
Zigzag	20	0.17	0.187
Co angular	200	0.096	0.113
Zigzag	200	0.100	0.108